EVIDENCE OF HIGH-ANGLE EJECTA FROM IMPACTS INTO VARIOUS GRANULAR MATERIALS.

C. J. Cline II[1] and M. J. Cintala[2]. [1]Jacobs, NASA Johnson Space Center, Houston, TX 77058 (christopher.j.cline@nasa.gov), [2]Astromaterials Research and Exploration Science Division, NASA Johnson Space Center, Code XI3, Houston, TX, 77058, USA.

Introduction: The dominant mechanism for resurfacing airless bodies is the excavation and ejection of material during the formation of impact craters. Ejecta that is deposited proximal to the rim of craters formed in the gravity-regime (where gravitational forces are greater than material strength) form a relatively smooth and continuous deposit. Aside from far-field secondary craters, craters observed on continuous ejecta deposits are mostly assumed to be representative of the primary impactor flux after the time of deposition. Sustained primary bombardment should produce a homogeneous crater population across this surface, thus providing an opportunity to determine crater size-frequency distributions and surface chronologies [1-3]. Deviations from this ideal have been observed as different crater-size distributions appearing between the continuous deposits and their superimposed melt ponds [4]. Numerous explanations for this discrepancy have been proposed, one of which is the occurrence of self-secondary craters, which would be created by ejecta launched at sufficiently high-angles to re-impact the fresh continuous ejecta deposits [1,5-7]. Here, we present results from cratering experiments to explore the influence of density, porosity, and friction on ejecta kinematics and report on the observation of such high-angle ejecta in cohesionless granular targets.

Methods: Experiments were carried out using the vertical gun in the Experimental Impact Laboratory at the NASA Johnson Space Center. Cylindrical PVC target containers (26.2 cm diameter, 12.2 cm depth) were filled with one of four different cohesionless sands (quartz, alumina, garnet, and olivine) that all had similar grain-size distributions and represent a range of intrinsic grain densities from 2.65 to 3.95 g cm^3. Each target was packed by either gently pouring the sand to generate a relatively lower-density/higher-porosity target, or by passing the sand through a sieve to create a higher-density/lower-porosity granular target. With this combination, a total of eight targets were created; each having a porosity of either 0.36±0.01, 0.45±0.01, or 0.53±0.01.

All experiments were conducted under near-vacuum (1 torr) conditions with 4.76-mm aluminum projectiles that impacted normal to the target surface at 1.55±0.03 km s^{-1}. The resulting crater morphometry was derived from data obtained with a 3D-scanner.

Ejecta kinematic data were collected using the Ejection-Velocity Measurement System (EVMS), originally detailed in [8]. This system records the velocity distribution of ejecta by means of a vertically oriented laser sheet. Triggered at the time of impact, the laser is pulsed at a predetermined rate, which sequentially illuminates the exterior edge of the expanding ejecta curtain. Each experiment is documented in a time exposure by a camera that is mounted outside of the impact chamber, thus producing a time-resolved image of the ejecta plume (Fig. 1). Parabolic fits are then applied to the digitized ejecta trajectories, yielding values of radial ejection position, ejection angle, and speed of the ejected particles.

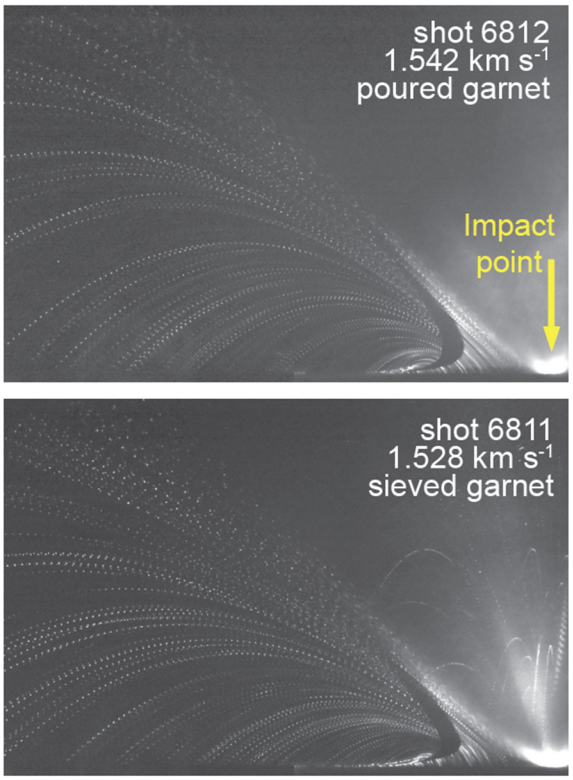

Figure 1. EVMS photographs showing the time-resolved ejecta from two targets made of the same garnet sand at higher (top panel) and lower (bottom panel) porosities (and bulk densities).

Results: Crater morphology was pronouncedly influenced by the target-fabrication method. Regardless of bulk density, craters formed in higher-porosity, poured-sand targets all had a simple, conical shape. In the lower-porosity sieved-sand targets (higher packing density and higher friction), however, all of the craters exhibited flat floors and small incipient central mounds. Craters in these denser targets also had consistently smaller rim heights, less voluminous rims, considerably

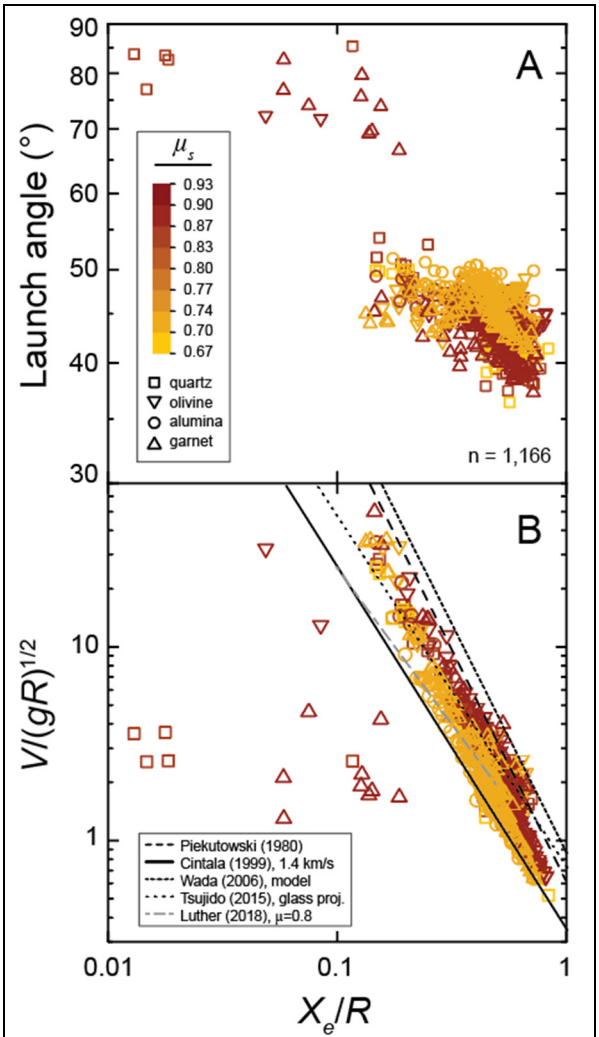

Figure 2. Launch angle (A) and scaled ejection speed (B) plotted as a function of launch position normalized by the crater radius. Data are for all eight shots and are colored according to the target's coefficient of static friction (μs). Sieved targets have higher friction coefficients and thus are shades of red, where poured targets appear as yellow symbols.

less interior volume, and a quantity of crushed target material resting on the crater floor, which was found buried below the impact point in the higher-porosity targets.

Ejecta characteristics were similarly influenced by the target fabrication method and the concomitant changes in physical properties. The ejection angles and speeds determined for poured targets, in general, were similar to those reported by other authors using granular materials, with higher speeds and launch angles in proximity to the impact point, decreasing as the rim is approached [8-11]. The ejecta from impacts into the sieved targets, for the most part, followed the same predictable power laws, but had lower ejection angles and higher speeds for a given normalized ejection position. Some ejecta from these more densely packed targets fall into a sample that had distinctively high launch angles (70-85°) and relatively low speeds (Figs. 1 and 2).

Discussion: The EVMS technique has been used to determine the speeds of ejecta, but it can also provide information on relative timing during the event. A gap in the laser strobing sequence is used to demarcate different strobing rates used during a single experiment. Since the trajectories of these high-angle ejecta contain more images of individual particles than the number of flashes in the first sequence (with no visible gap being present), these particles must have been launched after the first strobing sequence was complete, around 12 ms after impact.

The point-source assumption has been demonstrated to scale impact phenomena from near the crater rim crest to only one projectile radius from the impact point [10,12]. The data in Fig. 2 show that these high-angle ejecta are not described by current scaling laws despite sharing values of scaled launch position with the "well-behaved," lower-angle trajectories (right side of Fig. 2B). This suggests that the deviation from the scaling relations for these high-angle ejecta is not purely the consequence of proximity to the impact point.

Identifying the exact mechanism and/or mechanical property of the targets that is responsible for creating the observed high-angle ejecta is still under active investigation, but the implications for self-secondary crater production are clearly evident. Parabolic reconstructions of trajectories from these ejecta show secondary impacts occurring at radial positions ranging from inside the crater rim to as far as eight crater radii from the impact point, with multiple impacts occurring on the continuous ejecta deposit. More importantly, the relative timing of these self-secondary impacts is later than the time of deposition of the more "predictable" ejecta that constitute the continuous ejecta blanket.

References: [1] Shoemaker E. M. et al. (1969) *Surveyor Prog. Res., SP-184*, 19-128. [2] Neukum G. and König B. (1976) *LPSC XIII*, 2867-2881. [3] Neukum G. (1983) Univ. München, Munich, Germany, 186 p. [4] Hiesinger H. (2012) *JGR, 117*. [5] Strom R. G. and Fielder G. (1968) *Nature, 21,* 611-615. [6] Plescia J. B. and Robinson M. S. (2019) *Icarus, 321,* 974-993. [7] Zanetti M. et al. (2017) *Icarus, 298*, 64-77. [8] Cintala M.J. *et al.* (1999) *Meteoritics and Planetary Sci.* 34, 605-623. [9] Piekutowski A. J. (1980) *LPSC XI*, 2129-2144. [10] Housen K. R. and Holsapple K. A. (2011) *Icarus, 211*, 856-875. [11] Tsujido S. et al. (2015) *Icarus, 262,* 79-92. [12] Holsapple K. A. (1993) *Annu. Rev. Earth Planet. Sci., 21*, 333-373.